NASA CR-54126
EOS Report 4761-Final



# ANALYTICAL AND EXPERIMENTAL STUDIES OF SURFACE IONIZATION

by

W. D. Dong

prepared for

NATIONAL AERONAUTICS AND SPACE ADMINISTRATION

CONTRACT NAS3-5244

EOS ELECTRO-OPTICAL SYSTEMS, INC., PASADENA, CALIFORNIA
A Subsidiary of Xerox Corporation

NOTICE

This report was prepared as an account of Government sponsored work. Neither the United States, nor the National Aeronautics and Space Administration (NASA), nor any person acting on behalf of NASA:

A.) Makes any warranty or representation, expressed or implied, with respect to the accuracy, completeness, or usefulness of the information contained in this report, or that the use of any information, apparatus, method, or process disclosed in this report may not infringe privately owned rights; or

B.) Assumes any liabilities with respect to the use of, or for damages resulting from the use of any information, apparatus, method or process disclosed in this report.

As used above, "person acting on behalf of NASA" includes any employee or contractor of NASA, or employee of such contractor, to the extent that such employee or contractor of NASA, or employee of such contractor prepares, disseminates, or provides access to, any information pursuant to his employment or contract with NASA, or his employment with such contractor.

Requests for copies of this report should be referred to

National Aeronautics and Space Administration
Office of Scientific and Technical Information
Attention: AFSS-A
Washington, D.C. 20546

NASA CR-54126
EOS Report 4761-Final

FINAL REPORT

# ANALYTICAL AND EXPERIMENTAL STUDIES OF SURFACE IONIZATION

by

W. D. Dong

prepared for

NATIONAL AERONAUTICS AND SPACE ADMINISTRATION

1 September 1965

CONTRACT NAS3-5244

Technical Management
NASA Lewis Research Center
Cleveland, Ohio 44135
Spacecraft Technology Division
Yale E. Strausser

ELECTRO-OPTICAL SYSTEMS, INC.
A Subsidiary of Xerox Corporation
300 North Halstead Street
Pasadena, California 91107

# ANALYTICAL AND EXPERIMENTAL STUDIES OF SURFACE IONIZATION

by

W. D. Dong

## ABSTRACT

32597

Analytical studies and experimental measurements were made which resulted in the conclusion that rhodium and rhenium are better cesium-ionizer materials than tungsten for surface ionization engines. Other materials evaluated were iridium, tantalum, 74% tungsten-26% rhenium and 10% tungsten-90% tantalum. The conclusion was primarily based on an evaluation of critical temperature, work function and ionization efficiency. Also measured were atom and ion lifetimes and atom and ion desorption energies. A recommendation is made that gas contamination be the subject of future studies if the advantage of low critical temperature, such as that possessed by rhodium, is to be utilized. author

CONTENTS

ILLUSTRATIONS

## SUMMARY

An atomic cesium beam was used to study surface ionization on iridium, rhenium, rhodium, tantalum, tungsten, 10 percent tungsten-90 percent tantalum, and 74 percent tungsten-26 percent rhenium wires under vacuums of $10^{-9}$ torr and lower. The present program was motivated by a need to find materials superior in performance to that of tungsten for the surface ionization source in an ion engine.

Parameters evaluated were vacuum electron work functions, critical temperatures, atom and ion lifetimes, atom and ion desorption energies, and ionization efficiency. In the following summary of results, the more desirable materials are given first. The most important parameters for surface ionization engines are critical temperature and neutral fraction. The study indicated the order of increasing critical temperature to be

$$Ir < Rh < Re, W < \text{alloys} < Ta$$

and the order of decreasing work function to be

$$Rh > Re > W > W\text{-}Re > W\text{-}Ta > Ir > Ta$$

When ordered as to decreasing ionization efficiency (increasing neutral fraction),

$$Re > W > \text{alloys} > Rh > Ir > Ta$$

Both rhodium and rhenium have better surface ionization characteristics for ionizers than tungsten does. Attention is called to rhodium because of its low critical temperature ($740^{\circ}K$). However, we believe rhodium is more susceptible to gas contamination, and recommend that gas contamination on cesium surface ionization, particularly with rhodium, be a subject for future study.

# 1. INTRODUCTION

This is a summary report of an experimental and analytical study of cesium surface ionization conducted for the National Aeronautics and Space Administration by Electro-Optical Systems, Inc. The program, conducted from 24 January 1964 to 30 September 1964 under contract NAS3-5244, was motivated by a need to find materials superior in performance over that of tungsten for the ionization source of a surface ionization engine. This work was one aspect of a more general program pertaining to cesium surface ionization and the effect of gas contamination to the process[1,2]

An atomic beam technique was used to study cesium surface ionization on the following materials: iridium, rhenium, rhodium, tantalum, tungsten, 10 percent tungsten-90 percent tantalum, and 74 percent tungsten-26 percent rhenium. Before the admission of cesium to the system, vacuum work function measurements were taken. Ionization measurements used several different methods. Some of the ionization efficiencies were measured in a manner similar to that of Datz and Taylor in their work with alkali beams on platinum and tungsten[3]. Other ionization efficiencies were obtained by alternating the ion collecting field as did Starodubtsev[4]. Atom and ion lifetimes and atom and ion desorption energies were obtained both by the alternating field method, as used by Evans[5] and refined by Starodubtsev[4], and by the modulated beam technique employed by Hughes and Levinstein in their work with rubidium on tungsten[6]. Critical temperature measurements were made using a steady beam, since one of the incidental objectives of the present program was to evaluate the beam technique for such high-coverage phenomena.

## 2. APPARATUS

The cesium beam apparatus, shown in Fig. 1, housed two samples and one tungsten standard in vacuum. A small oven (Fig. 1) supplied a beam of cesium vapor to the samples. The beam was collimated to strike each of the three filaments with the same flux intensity except for a small angular distribution factor. Cesium atoms ionized on the wire surface were drawn, under the influence of a 22-1/2 volt potential, to either the cylindrical collector or guard surrounding the wire. This battery-supplied voltage was sufficient to collect the ions in the emission-limited mode. The guard insured a radial electric field between collector and filament so that the collector intercepted only ions desorbing from a = 0.04142 $cm^2$ of area on the filament. From the collector, connection was made to either a Keithley 600A Electrometer, a Tektronix oscilloscope with a Type D preamplifier, or a Varian Model F-80 X-Y recorder, depending on the sensitivity and time response required. Both guard and vacuum chamber were maintained at ground potential. The voltage of the collector was determined by the voltage across the input resistor of the measuring instrument, generally a fraction of a volt positive with respect to ground. Power to the filaments was supplied by regulated power supplies. Filament voltage and current were monitored with 1/4 percent Greibach meters.

The vacuum chamber, which could be baked to speed outgassing, was constructed of stainless steel with metallically sealed glass view ports. It was evacuated by a 4-inch National Research Corporation Model HS4-750 diffusion pump through a special anti-oil-creep, optically dense bakeable liquid nitrogen trap. The preparation and pump-down procedure described in Appendix A is sufficient to reach a base vacuum of $4 \times 10^{-10}$ torr consistently. The diffusion pump was in turn evacuated through a refrigerated foreline trap by a Welch Duoseal

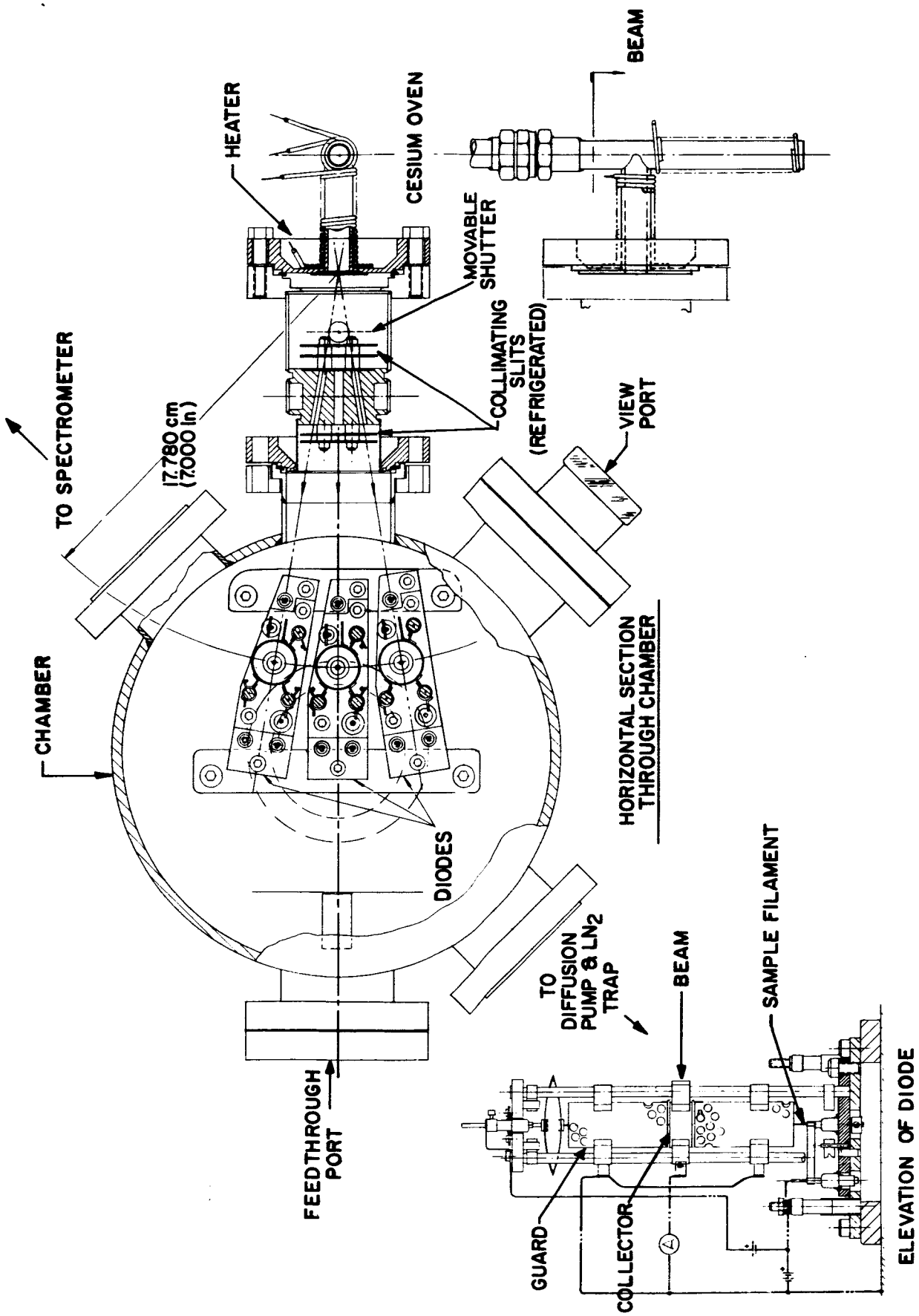


FIG. 1 CESIUM BEAM APPARATUS

425 ℓ/min. mechanical pump. Vacuum was indicated by a NRC 551A-P ion gage located between the vacuum chamber and the liquid nitrogen trap. The actual vacuum in the chamber is probably a factor of 2 or so higher than indicated by the gage. Composition of the residual background gas was monitored by a glass-enclosed General Electric Residual Gas Analyzer mounted at one side of the vacuum chamber. Mass spectra obtained are discussed in Appendix B.

## 3. ANALYSIS

### 3.1 Vacuum Electron Work Function

When a metal is at temperature T, the current density of electrons leaving the metal is given by the Richardson-Dushman equation[7]

$$J = A^{**} T^2 e^{-\varphi^{**}/kT} \quad (1)$$

$A^{**}$ is the Richardson constant and $\varphi^{**}$ is the Richardson work function for polycrystalline materials. If $A^{**}$ is set equal to 120 amps/cm$^2$-deg$^2$, the value for an idealized metal, the $\varphi^{**}$ becomes the effective work function $\varphi_e$. Consequently $\varphi^{**}$ and $\varphi_e$ are related by[7]

$$\varphi_e = \varphi^{**} + \frac{T}{5040} \log_{10} \frac{120}{A^{**}} \quad (2)$$

Use of this relation will be made later.

We evaluated $\varphi^{**}$ and $A^{**}$ for each material by plotting $\log_{10} J/T^2$ versus $10^4/T$. The value of J was obtained by dividing the electron collector current by the area a. The true temperature T in degrees Kelvin was obtained from optical pyrometer readings of the brightness temperature of the sample, corrected for emissivity as described in Appendix C.

For the iridium, rhodium, tungsten and alloy samples the possibility of contamination due to residual background gas at sample temperatures below about 1800°K was minimized by flashing the filament to 1800°K before each electron emission reading and by maintaining the vacuum in the $10^{-10}$ torr range for the majority of the readings.

These precautions did not seem to be necessary for rhenium or tantalum. In the absence of contamination the points of the $\log_{10} J/T^2$ plot versus $10^4/T$ plot, according to Eq. 1 lie in a straight line, the slope of which multiplied by 1.984 is $\varphi^{**}$ and with an ordinate intercept of $\log_{10} A^{**}$. All the samples had straight line plots similar to those for tantalum. (See Fig. 2.) The corresponding $\varphi^{**}$ and $A^{**}$ for each plot is given in Table 1.

TABLE 1

VACUUM THERMIONIC CONSTANTS

| Material | Reference | Configuration | $\varphi^{**}$ (eV) | $A^{**}$ (amps/cm$^2$-deg$^2$) |
|---|---|---|---|---|
| Iridium | Present Work | Wire | 4.22 ± 0.11 | 94 |
| | Ref 8 | Ribbon | 5.40 | 170 |
| | Ref 9 | Wire | 5.3 | 100 |
| Rhenium | Present Work | Wire | 4.78 ± 0.13 | 47* |
| | Ref 10 | Wire | 4.72 | 17 |
| | Ref 11 | Wire | 4.74 | 720 |
| | Ref 12 | Ribbon | 5.09 | 760 |
| Rhodium | Present Work | Wire | 4.89 ± 0.13 | 41 |
| | Ref 9 | Wire | 4.9 | 100 |
| | Ref 13 | Ribbon | 4.8 | 33 |
| Tantalum | Present Work | Wire | 4.12 ± 0.11 | 35‡ |
| | Ref 14 | Wire | 4.19 | 55 |
| Tungsten | Present Work | Wire | 4.71 ± 0.13 | 148 |
| | Ref 15 | Wire | 4.52 | 72 |
| 10% W-90% Ta | Present Work | Wire | 4.34 ± 0.12 | 360 |
| 74% W-26% Re | Present Work | Wire | 4.52 ± 0.12 | 65 |

*The value reported in EOS Report 4761-ML-2 was a typographical error.
‡Recomputed value supersedes that reported in EOS Report 4761-ML-2.

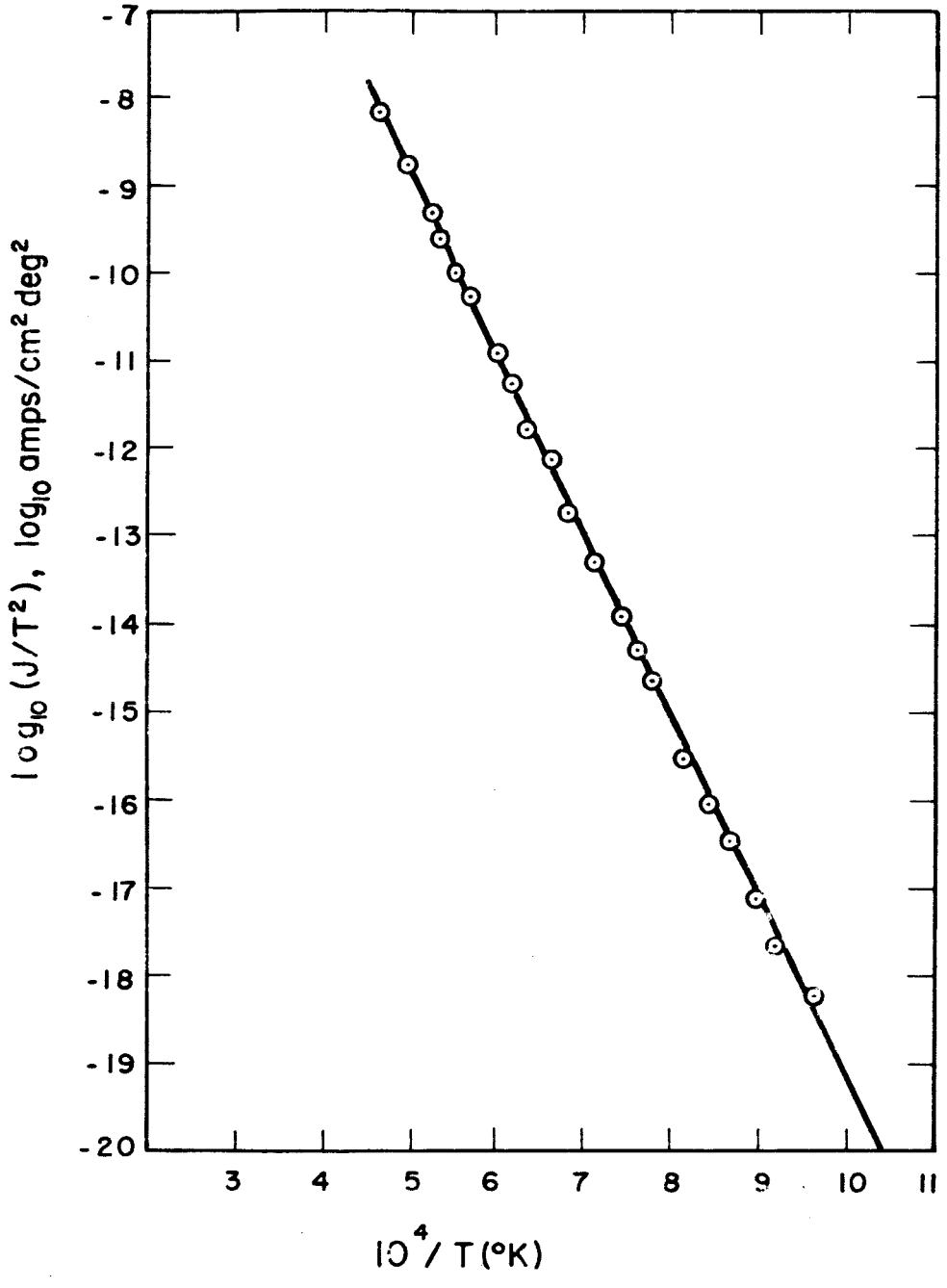


FIG. 2 ELECTRON EMISSION FROM A TANTALUM SAMPLE

These electron emission measurements were taken prior to the admission of cesium into the vacuum system. Before taking the data the filaments were aged for a period of 1 to 5 hours at a maximum temperature that did not result in permanent elongation of the wires. The resistance and electron emission were monitored during aging to determine when a stable condition had been reached.

Equation 1 is valid only under emission-limited conditions; consequently, the filament was biased 500 volts negative with respect to the collector for the electron emission data. The current-voltage characteristic was flat at this voltage for all currents encountered.

The work function error shown in Table 1 is a systematic error, reflecting the inaccuracies of the instruments and the uncertainties in the emissivity calibration as discussed in Appendix D. All our results have been obtained by fitting the points to a straight line using the method of least squares. In every case in which the random error was computed, it was found to be less than the systematic error. For example, the random error for the rhenium specimen was $\Delta\varphi^{**} = \pm 0.04$ eV as compared with the above systematic error $\Delta\varphi^{**} = \pm 0.10$ eV. The systematic error in $A^{**}$ is estimated to be on the order of $A^{**}$ itself, hence is not listed in Table 1.

Generally we found the random error for a given filament to be small, yet another filament made from the same lot of wire and aged until stable, though of course in not exactly the same way, might give different results. For example, another rhenium filament yielded 5.15 eV and 760 amps/cm$^2$-deg$^2$.[2] In the case of tungsten the difference was not as striking. Three other tungsten filaments yielded 4.72 eV and 66 amps/cm$^2$-deg$^2$[2], 4.57 eV and 52 amps/cm$^2$-deg$^2$, and 4.69 eV and 100 amps/cm$^2$-deg$^2$ in the present program.

The corresponding effective work function values of the Richardson work function values reported in Table 1 are calculated by Eq. 2 to be those of Table 2, in anticipation of their need in Section 3.6.

TABLE 2

EFFECTIVE WORK FUNCTION AT 1000°K

| Material | $\varphi_e$ (eV) |
|---|---|
| Iridium | 4.24 |
| Rhenium | 4.86 |
| Rhodium | 4.98 |
| Tantalum | 4.23 |
| Tungsten | 4.69 |
| 10% W-90% Ta | 4.25 |
| 74% W-26% Re | 4.57 |

### 3.2 Critical Temperature

The temperature at which the ion emission decreases rapidly from an emission-limited plateau as the sample temperature is lowered is called the lower critical temperature, while the temperature at which ion emission increases rapidly to the emission-limited plateau as the sample temperature is raised is called the upper critical temperature. Experiments having cesium vapor in thermal equilibrium with the chamber walls have a transition from the nonemission to the emission state that is nearly discontinuous.[16] In the present experiment where the coverage is not necessarily uniform the transition is more gradual. A typical case is shown in Fig. 3. Consequently we specified in our analysis, the lower critical temperature to be that temperature at which the ion current has dropped to 90 percent of its plateau value and the upper critical temperature to be that temperature at which the ion current has reached 10 percent of its plateau value. However, we were unable to assign separate values for upper and lower critical temperatures because of the scatter in the data; consequently, Table 3 reports only one approximate critical temperature for each sample.

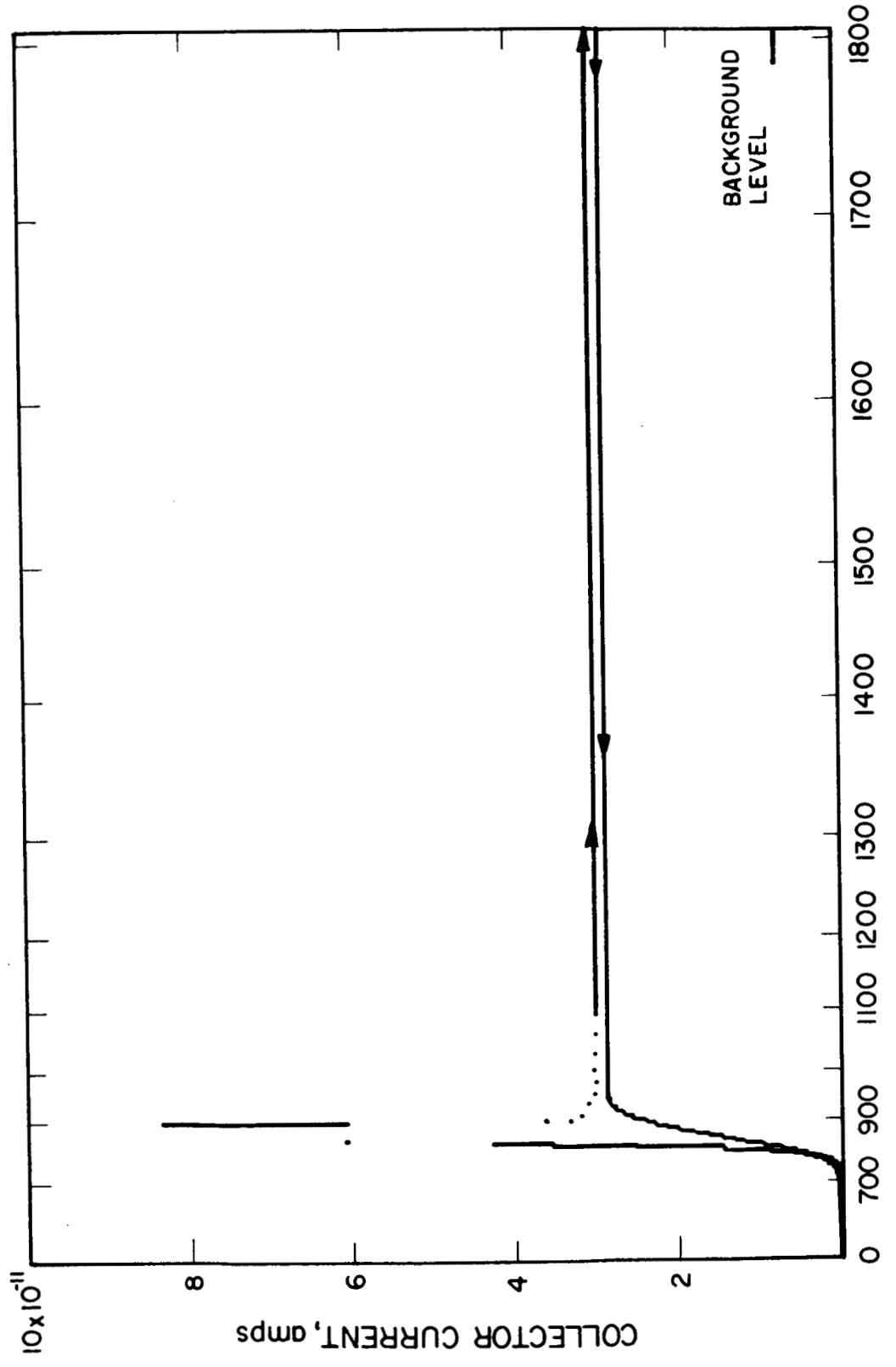


FIG. 3 $Cs^+$ COLLECTOR CURRENT FROM A 90% W-10% Ta ALLOY VS ALLOY TEMPERATURE

TABLE 3

CESIUM CRITICAL TEMPERATURES

| Material | Atom Flux $\mu_a$ (atoms/cm$^2$-sec) | Critical Temperature ($^\circ$K) |
|---|---|---|
| Iridium | $10^{10}$-$10^{13}$ | 660 ± 30 |
| Rhenium | $10^{8}$ -$10^{11}$ | 800 ± 100 |
| Rhodium | $10^{11}$-$10^{12}$ | 740 ± 30 |
| Tantalum | $10^{8}$ -$10^{11}$ | 850 ± 30 |
| Tungsten | $10^{9}$ -$10^{10}$ | 800 ± 60 |
| 10% W-90% Ta | $10^{9}$ -$10^{11}$ | 810 ± 50 |
| 74% W-26% Re | $10^{9}$ -$10^{11}$ | 810 ± 40 |

The uncertainty in the critical temperature is the average deviation of a number of points from their mean. Within each range of $\mu_a$ (the incident cesium atom flux) given in Table 3, the scatter was such that we were unable to evaluate a dependence of critical temperature on $\mu_a$.

It was found that the lower critical temperature was reproducible within the scatter of the data, independent of the rate of temperature decrease for slow rates. However, the upper critical temperature was found to be dependent on the rate of temperature increase, even though the rate was quite slow. Furthermore, the upper critical temperature could be made to approach the lower critical temperature by increasing the temperature very slowly, of the order of 3 deg/min. Since no further investigations were made of this time dependence, the upper critical temperature that contributed to the values of Table 3 were obtained in the last manner.

### 3.3 Ion Desorption Time and Energy

When cesium atoms strike a hot metal surface, they do not reevaporate immediately, but spend a finite time on the surface before coming off as cesium ions. As a consequence of this, when a square pulse of cesium atoms is directed to a hot metal surface, the resulting ion signal rises and then decays exponentially. For high work function surfaces, the time constant of the rise or decay is the ion desorption time $\tau_p$. This phenomena affects contact ion engine efficiency for it is related directly to the energy required to desorb ions from a surface. The nature of this relationship is discussed in Section 3.3.3.

Quantitatively the sorption process can be described in terms of a change in the surface coverage $\sigma$ being equal to an incoming flux $\mu$ less the outgoing flux $\nu$ of atoms and ions[16], i.e.,

$$\frac{d\sigma}{dt} = \mu_a + \mu_p - \nu_a - \nu_p \qquad (3)$$

The subscript a and p denote atoms and ions, respectively. Equation 3 is a very general formulation for the rate of change of the coverage $\sigma$, which is expressed in atoms per unit surface area. In this experiment the flux of ions onto the wire is negligible, hence $\mu_p$ will always be zero. Furthermore when the coverage is less than $10^{12}$ atoms/cm$^2$, $\nu_a$ and $\nu_p$ are approximately

$$\nu_a = \frac{\sigma}{\tau_a} \quad \text{and} \quad \nu_p = \frac{\sigma}{\tau_p} \qquad (4, 5)$$

where $\tau_a$ and $\tau_p$ are independent of $\sigma$. Since in a beam experiment the coverage might vary with position, coverage, rigorously, should be regarded as averaged. Thus, to solve Eq. 3 one only needs to know the behavior in time of the incident atom flux ($\mu_a$). We anticipate the results by stating that the coverage $\sigma$ and, therefore, the measured

ion current will have an exponential time dependence whose characteristic time constant $\tau_p$ is the ion desorption time. The analysis, which follows a treatment by Worden using differential equations,[17] will be carried through for two different methods of varying $\mu_a$ to obtain $\tau_p$.

### 3.3.1 Desorption Time by Modulated Beam Method

When actuated by a magnetic coil, a shutter positioned between the filaments and the atomic cesium oven allows a nearly square pulse of cesium atoms to strike the filaments.[6] In the following analysis, it is shown that the resulting ion signal from the filament is a rising exponential followed by a decaying exponential whose characteristic time is called the ion desorption time $\tau_p$ (Fig. 4).

Let $\mu_a^b$ represent the incident atomic flux due to background cesium and $\mu_a^s$ be the incident atomic flux due to the cesium oven; then Eq. 3 with the shutter open becomes

$$\frac{d\sigma}{dt} + \frac{1}{\tau}\sigma = \mu_a^b + \mu_a^s . \tag{6}$$

When the shutter is closed, Eq. 3 is

$$\frac{d\sigma}{dt} + \frac{1}{\tau}\sigma = \mu_a^b . \tag{7}$$

We have written

$$\frac{1}{\tau} = \frac{1}{\tau_a} + \frac{1}{\tau_p} . \tag{8}$$

The corresponding solutions are

$$\sigma = \tau\,(\mu_a^b + \mu_a^s)\,(1 - e^{-t/\tau}) + \sigma^b\, e^{-t/\tau} \tag{9}$$

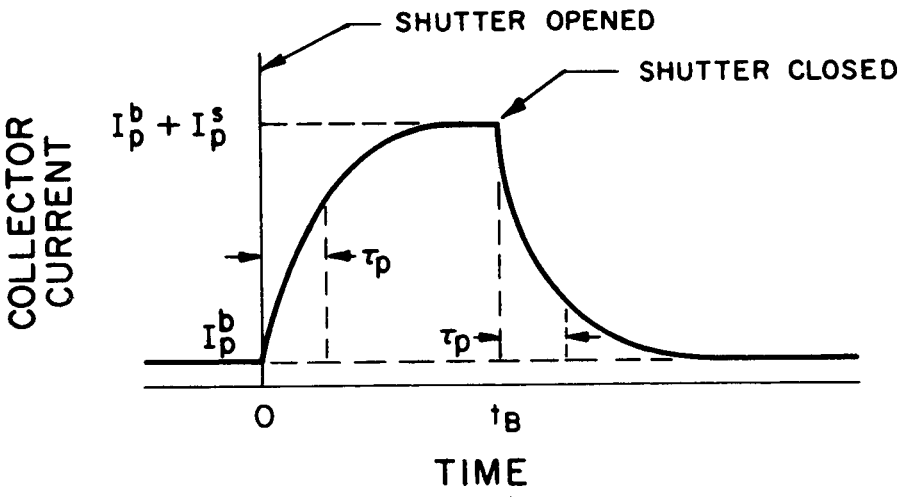


FIG. 4 OSCILLOSCOPE TRACE OF COLLECTOR CURRENT IN MODULATED BEAM METHOD

$$\sigma = \tau \mu_a + [\sigma^b - \tau (\mu_a^b + \mu_a^s) + \tau \mu_a^s e^{t_B/\tau}] e^{-t/\tau} \quad (10)$$

where $t_B$ is the time base of the square pulse of cesium atoms from the oven measured from the time at which the shutter was opened ($t = o$).

The ion and atom fluxes are related by the Saha-Langmuir equation[18]

$$\frac{\nu_p}{\nu_a} = \frac{\omega_p}{\omega_a} e^{(\varphi - V_i)/kT} \quad (11)$$

where $\varphi$ is the work function, T is the temperature of the surface, $V_i$ is the ionization potential of the adsorbed atoms, and $\omega_a$ and $\omega_p$ are the statistical weights of the atom and ion, respectively. When $\varphi > V_i$ in Eq. 11, as for cesium on tungsten, $\nu_p >> \nu_a$, or $\tau_p << \tau_a$, we may set $\tau$ equal to $\tau_p$ in the exponential of Eqs. 9 and 10. The error in doing so is less than the experimental error in measuring $\tau$.

The observed collector current $I_p$ is related to the coverage $\sigma$ by

$$I_p = e \nu_p A = eA\sigma/\tau_p ; \quad (12)$$

hence, during the time the shutter is open,

$$I_p = I_p^b + I_p^s (1 - e^{-t/\tau_p}) \qquad o \leq t \leq t_B \quad (13)$$

and during the time the shutter is closed

$$I_p = I_p^b + I_p^s (e^{t_B/\tau_p} - 1) e^{-t/\tau_p} . \qquad t_B \leq t \quad (14)$$

$I_p^b$ is the ion current from the sample due to the background cesium and $I_p^s$ is the steady ion current from the sample due to the oven. To write the currents in this form we made use of $\beta = \frac{\tau}{\tau_p}$ and then $\upsilon_p = \beta\mu_a$.

The background cesium $I_p^b$ is seen to contribute to the total ion signal by a constant amount as one might expect. The ion signal due to the oven is seen to have an exponential behavior whose time constant $\tau_p$ is the desired ion desorption time at a given surface temperature.

Accuracy in the determination of $\tau_p$ suffers when the background contribution $I_p^b$ is comparable to the oven contribution $I_p^s$ because of fluctuations in $I_p^b$. When this is the case, better results are obtained using the alternating field technique which yields not only $\tau_p$ but also $\beta$.

### 3.3.2 Desorption Time by Alternating Field Method

No shutter is used; instead, in this method, the transient phenomenon is obtained by alternating the polarity between the collector and the sample surface.[4,5] When the collector is positive with respect to the sample, no positive ions can leave the sample and the coverage is higher than if the polarity were reversed. When the polarity is reversed positive ions can leave the filament surface; therefore, $\upsilon_p$ immediately rises to a value corresponding to the coverage $\sigma$ just before the polarity was reversed. However, because ions now are being desorbed, the coverage $\sigma$ decreases. Fig. 5 shows this behavior in terms of collector current signal. It is not necessary that the coverage reach a steady state value before switching the field to determine $\tau_p$.

The coverage during the ion collecting part of the cycle is described by

$$\frac{d\sigma}{dt} + \frac{1}{\tau}\sigma = \mu_a \ , \qquad (15)$$

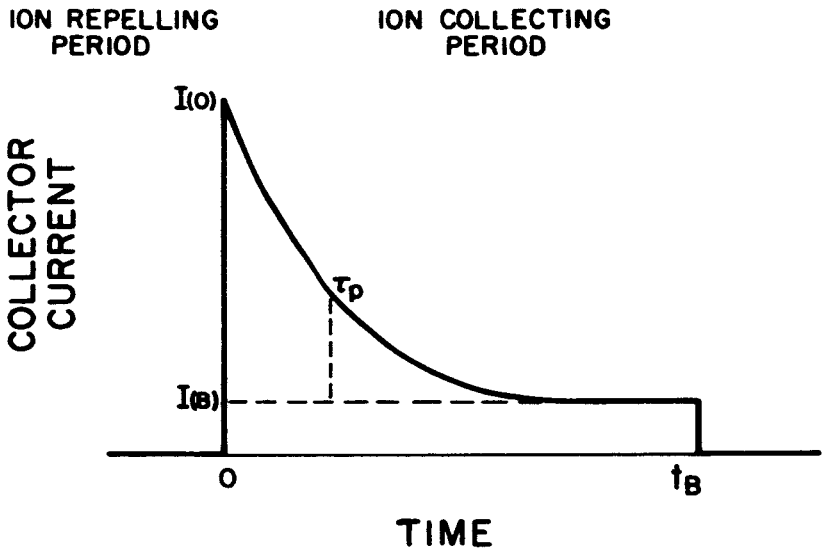


FIG. 5 OSCILLOSCOPE TRACE OF COLLECTOR CURRENT IN ALTERNATING FIELD METHOD

while during the ion repelling portion the coverage is

$$\frac{d\sigma}{dt} + \frac{1}{\tau_a}\,\sigma = \mu_a \tag{16}$$

where as before $\tau$ is defined by Eq. 8. One does not need to discriminate here between atomic cesium background and incident atomic cesium fluxes. The respective solutions are

$$\sigma = \mu_a\tau + \left[\frac{\sigma(0)}{\tau_p} - \mu_a\tau\right] e^{-t/t_B}, \qquad 0 \le t \le t_B \tag{17}$$

and

$$\sigma = \mu_a\tau_a + \left[\sigma(B) - \mu_a\tau_a\right] e^{-(t-t_B)/\tau_a}, \qquad t_B \le t. \tag{18}$$

$\sigma(0)$ is the coverage at the time at which the field is switched to ion collecting and $\sigma(B)$ is the coverage at the time $t_B$ at which the field is switched back to ion repelling. If $t_B$ is long enough to establish a steady state coverage, then by approximating $\tau$ by $\tau_p$ for the same reasons listed in Section 3.3.1, and using Eq. 12 again, the observed collector current is

$$I_p = I_p(\infty) + \left[I_p(0) - I_p(B)\right] e^{-t/\tau_p}. \tag{19}$$

Thus, when the field is switched to ion collecting, the ion signal rises almost instantaneously and then decays exponentially to a steady state current $I_p(\infty)$ with a characteristic time $\tau_p$ when displayed on an oscilloscope.

3.3.3 Ion Desorption Energies

Having obtained the ion desorption time $\tau_p$ as a function of temperature, one can then evaluate the ion desorption energy $Q_p$, which an ion must acquire before it can escape from the metal

surface. According to reaction rate theory the desorption time $\tau_p$ is described by

$$\tau_p = \tau_{po} e^{Q_p/kT} \tag{20}$$

where $\tau_{po}$ is a constant, independent of the temperature T. Thus a plot of $\log_{10} \tau_p$ versus $10^4/T$ would result in a straight line whose slope times 1.9814 is $Q_p$ and whose intercept is the logarithm of $\tau_{po}$. This is indeed the case as Figs. 6 and 7 illustrate. The points began to deviate from the straight line abscissa values below 1000°K as the ion desorption time becomes comparable to the electronic circuit time constant, which is between 0.4 and 0.9 millisec, depending on the filament used.

### 3.3.4 Results

The majority of the ion desorption times was obtained by the Alternating Field Method; however, some data were obtained by the Modulated Beam Method. The procedure in using the Alternating Field Method was to accumulate for a time sufficient to reach a steady state coverage before reversing the field to obtain the $I_o$ signal. Ion desorption times for iridium, rhodium, tungsten and 10 percent W-90 percent Ta were obtained in this manner, except for the top two circled points of the last alloy (Fig. 8) where the filament had to be flashed to 1600°K before accumulating, in order to obtain exponential decay curves. Ion desorption times obtained by the Modulated Beam Method yielded results which were consistent with the Alternating Field Method.

When the Alternating Field Method was applied to the 74 percent W-26 percent Re sample, nonexponential decay curves were observed unless the filament was first flashed to 1800°K before accumulating. In attempting to evaluate the accumulation time required for a steady state coverage to be reached, we found that the

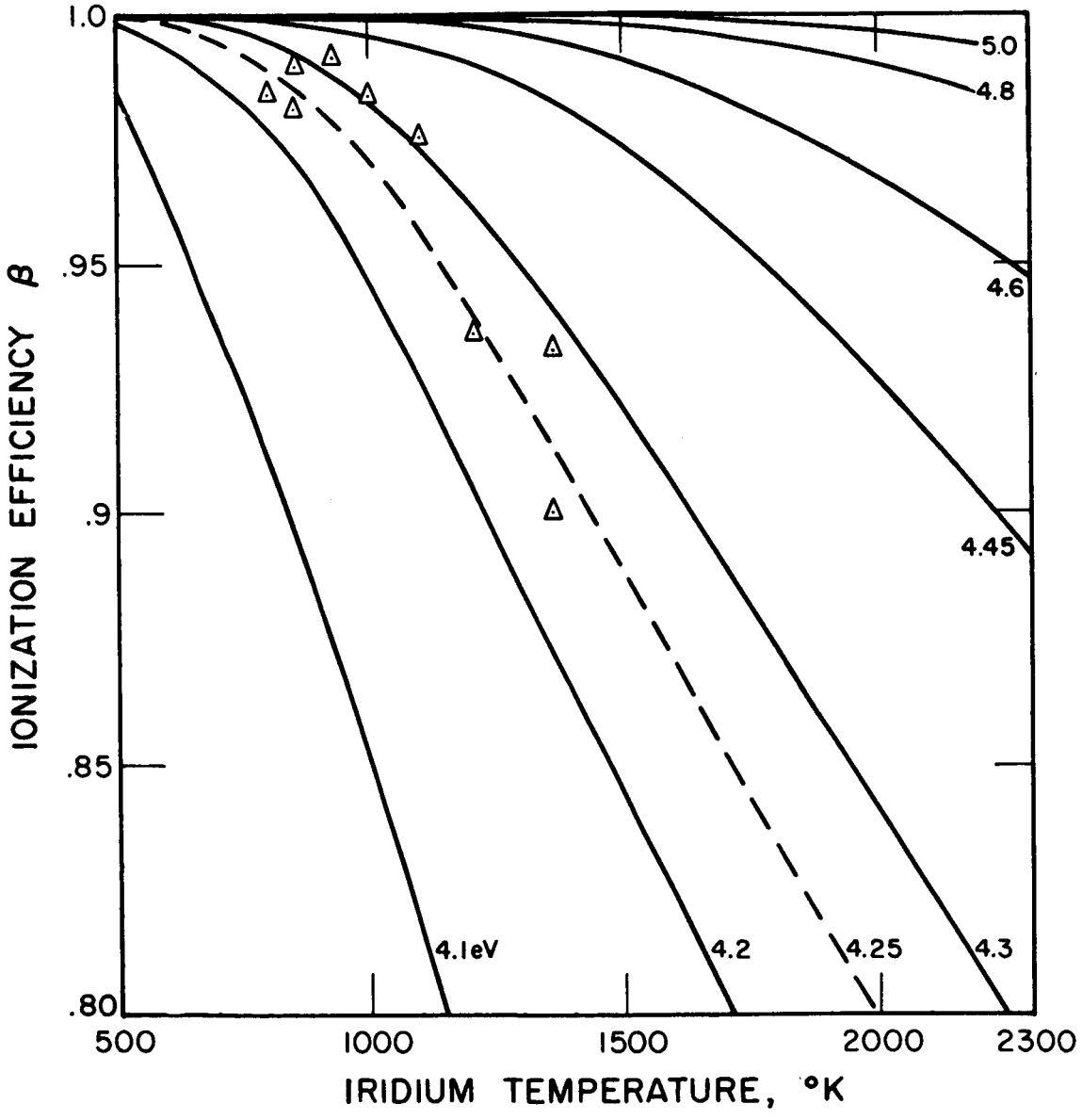


FIG. 6 $Cs^+$ IONIZATION EFFICIENCY VS IRIDIUM TEMPERATURE

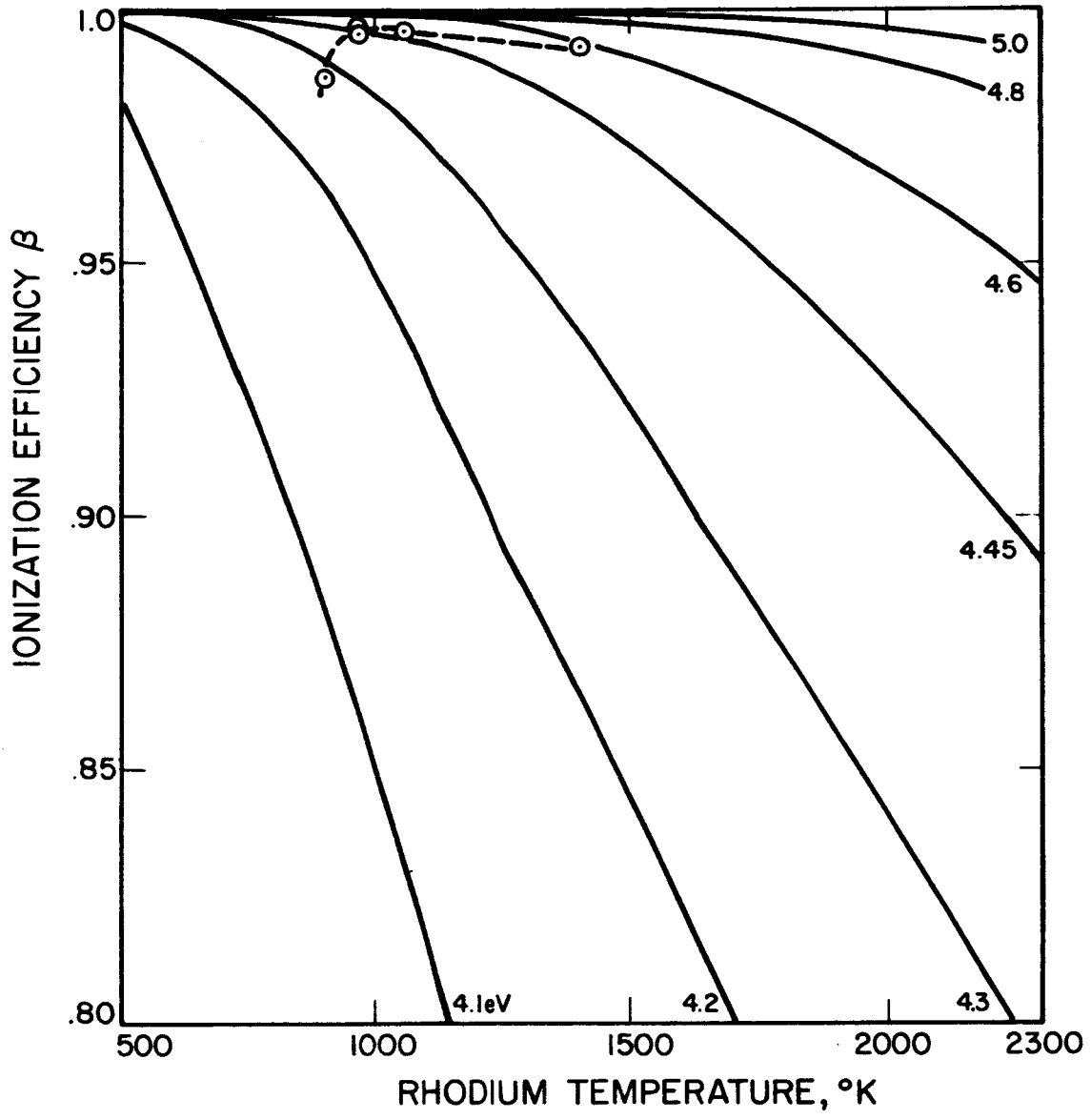


FIG. 7 $Cs^+$ IONIZATION EFFICIENCY VS RHODIUM TEMPERATURE

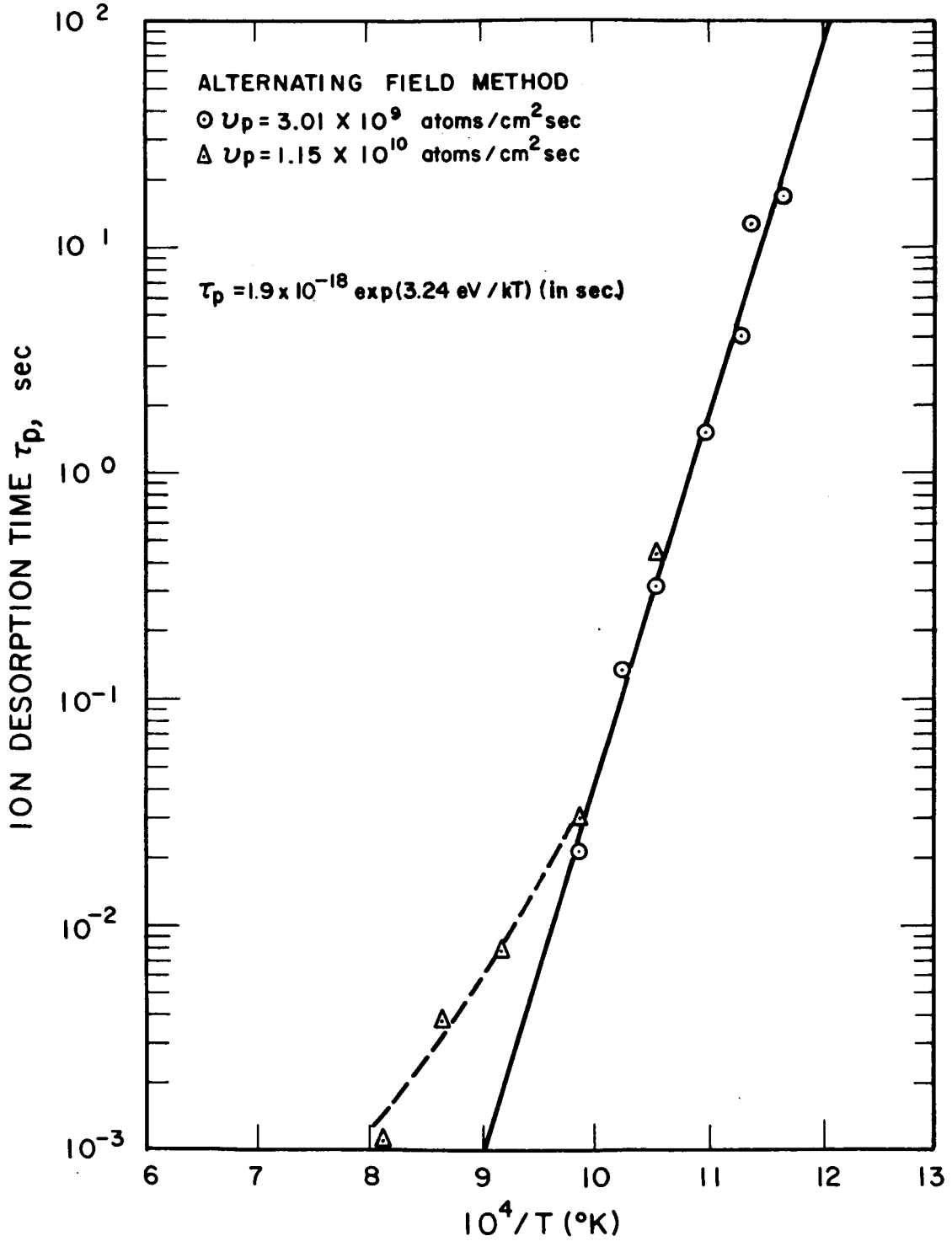


FIG. 8 $Cs^+$ DESORPTION TIME VS 1/T FOR A 10% W-90% Ta ALLOY

$I_o$ signal at first increases with accumulation time and then levels out, the ion desorption time remaining constant. However, at longer accumulations times the $I_o$ signal begins to decrease and the ion desorption time begins to increase. It was as if one were seeing a contamination layer with a long desorption time building up on the surface. As pointed out in Section 3.3.2, it is not necessary to reach a steady cesium coverage in the ion repelling mode for desorption time measurements. Consequently, the accumulation time for this alloy was fixed as 2 minutes which is short compared to the time, 15 minutes, when the contamination effect began to become important.

After observing this decrease in $I_o$ with long accumulation times, we examined tungsten and the 10 percent W-90 percent Ta alloy for this behavior. They exhibited similar effects though not as pronounced as the 74 percent W-26 percent Re alloy. We did not have an opportunity to check the iridium and rhodium ion desorption data; however, we believe the large scatter encountered for iridium is due to a strong contamination effect of this type. The rhodium data did exhibit deviations from the expected exponential decay.

Results for the ion desorption times are summarized in Table 4 as the ion desorption energy $Q_p$ and the preexponential $\tau_{po}$ occurring in Eq. 20. No values of $Q_p$ and $\tau_{po}$ are quoted for iridium because of the previously mentioned scatter. Iridium ion desorption time was about 0.02 sec at 850°K.

TABLE 4

CESIUM ION DESORPTION ENERGIES AND TIMES

| Material | Reference | $Q_p$ (eV) | $\tau_{po}$ (sec) |
|---|---|---|---|
| Iridium | Present Work | See text | |
| Rhodium | Present Work | 3.25 ±0.11 | $1.1 \times 10^{-19}$ |
| Tungsten | Present Work | 2.79 ±0.09 | $3.3 \times 10^{-17}$ |
| | Ref. 19 | 3.60 | $4.0 \times 10^{-17}$ |
| | Ref. 20 | 2.04 | $1.1 \times 10^{-12}$ |

Table 4 (contd)

| Material | Reference | $Q_p$ (eV) | $\tau_{po}$ (sec) |
|---|---|---|---|
| 10% W-90% Ta | Present Work | 3.24 ± .11 | $1.9 \times 10^{-18}$ |
| 74% W-26% Re | Present Work | 2.21 ± .08 | $1.3 \times 10^{-13}$ |

The uncertainty in $Q_p$ was computed as a systematic error in accordance with Appendix D. The method fails for $\tau_{po}$ because of the large error which we estimate to be approximately ±10 times the appropriate exponential, hence individual uncertainties for $\tau_{po}$ are not given. The number of points was not sufficient to make a meaningful standard deviation computation.

3.4 Atom Desorption Time and Energy

The accumulation time required to reach a steady state coverage is a measure of the atom desorption time $\tau_a$. Because of the contamination effect described in the previous section, this approach was not successful in obtaining reliable atom desorption times that could be used to compute an atom desorption energy according to

$$\tau_a = \tau_{ao} e^{+Q_a/kT}, \qquad (21)$$

which is of the same form as Eq. 20 and which is derived in the same way. Table 5 below shows that the atom desorption time is several to many orders of magnitude larger than the ion desorption time.

TABLE 5

CESIUM DESORPTION TIMES AT 1,000°K

| Material | $\tau_p$ measured (sec) | $\tau_a$ measured (sec) | $\tau_a$ from $\tau_p$, $\beta$ (sec) |
|---|---|---|---|
| Iridium | 0.002 | - | 0.06 |
| Rhodium | 0.0027 | - | 0.73 |
| Tungsten | 0.0040 | 72 | 40 |
| 10% W-90% Ta | 0.040 | 150 | 130 |
| 74% W-26% Re | 0.017 | 60-168 | 57 |

Measured values refer to those obtained directly by either the Modulated Beam or the Alternating Field Method. The last column of Table 5 is atom desorption time obtained from the ion desorption time and the ionization efficiency by

$$\tau_a = \frac{\beta}{1 - \beta} \tau_p \qquad (22)$$

which comes from Eqs. 4 and 5 and from the definition of $\beta$. Measured values (Subsection 3.5) were used for $\beta$. Table 5 also shows that the two values of $\tau_a$ obtained by different methods agree for a given material within a factor of two.

We use the conservation of energy equation

$$Q_a - Q_p = \varphi - V_i \qquad (23)$$

to evaluate $Q_a$. If $\varphi$ is the effective work function of Table 2 and the values of Table 4 are used for $Q_p$, then, using 3.893 eV as the ionization potential for cesium[21], we have the $Q_a$ of Table 6.

TABLE 6

CESIUM ATOM DESORPTION ENERGY

| Material | Reference | $Q_a$ (eV) |
|---|---|---|
| Rhodium | Present Work | 4.3 |
| Tungsten | Present Work | 3.6 |
| | Ref. 16 | 2.83 |
| 10%W-90% Ta | Present Work | 3.6 |
| 74%W-26% Re | Present Work | 2.9 |

3.5 Ionization Efficiency

The ionization efficiency $\beta$ is defined as the ratio of the number of ions from an ionizing surface to the number of atoms supplied, i.e.,

$$\beta = \frac{\upsilon_p}{\mu_a} \qquad (24)$$

There are several ways to measure $\beta$ for a material. Simplest in principle is to direct two identical beams, one of which goes to the sample wire, the other to a wire of known 100 percent efficiency. The two resulting ion currents are collected, measured, and their ratio taken to obtain $\beta$. This method works well when the incident beams are indeed identical, but more important, when the cesium background flux to the wire is also negligible compared to the beam flux. Since this was seldom the case, another method was used to obtain most of the $\beta$ values.

In the alternating field method discussed earlier, if one allows the coverage to reach a steady state value before changing the polarity, one has a way of measuring $\beta$. Suppose $\sigma_o$ represents the steady state coverage in the ion repelling mode up to time $t = 0$. Let the field polarity be changed to the ion collecting mode at $t = 0$, then the coverage $\sigma(t)$ will decrease to a new steady state value, which we call $\sigma_\infty$. In the ion repelling mode particles can only leave the filament as neutrals, hence the atom flux 'off' equals the atom flux 'on' or

$$\mu_a = \frac{\sigma_o}{\tau_a} = \frac{\sigma_o}{\tau_{ao}} e^{-Q_a/kT} \tag{25}$$

For the ion collecting mode both atoms and ions can leave the filament surface so that atom flux 'on' equals atom and ion flux 'off' or

$$\mu_a = \sigma_\infty \left( \frac{e^{-Q_a/kT}}{\tau_{ao}} + \frac{e^{-Q_p/kT}}{\tau_{po}} \right) \tag{26}$$

Eliminating $\mu_a$ between Eqs. 25 and 26 results in

$$\frac{\sigma_o}{\sigma_\infty} = 1 + \frac{\tau_{ao}}{\tau_{po}} e^{-(Q_p - Q_a)/kT} \tag{27}$$

Then using Eqs. 20, 21, and

$$\frac{\tau_{ao}}{\tau_{po}} = \frac{\omega_p}{\omega_a} \tag{28}$$

we have that

$$\frac{\sigma_o}{\sigma_\infty} = 1 + \frac{\omega_p}{\omega_a} e^{(\varphi - V_i)/kT} \tag{29}$$

Consequently $\beta$, with the aid of Eqs. 11 and 29, becomes

$$\beta = \frac{1}{1 + \frac{\sigma_\infty}{\sigma_o - \sigma_\infty}} = \frac{\sigma_o - \sigma_\infty}{\sigma_o} \quad . \tag{30}$$

Then using Eq. 12 the expression for the ionization efficiency is expressed in the useful form

$$\beta = \frac{I_o - I_\infty}{I_o} \tag{31}$$

Thus to measure $\beta$ the coverage is allowed to reach steady state with the collector in the positive mode. The collector polarity is switched to negative and the peak amplitude $I_o$ is noted on an oscilloscope or fast recorder. $I_\infty$ is the resulting steady state current in the negative collector mode. The ionization efficiency for iridium and rhodium had the most pronounced temperature dependence of all the samples, hence are presented in Fig. 6 and 7 respectively. The other samples had efficiencies that were nearly constant.

Table 7 lists the values of $\beta$ obtained by direct measurement and two indirect methods of independent calculation. The measured values for tantalum and rhenium were obtained by dividing

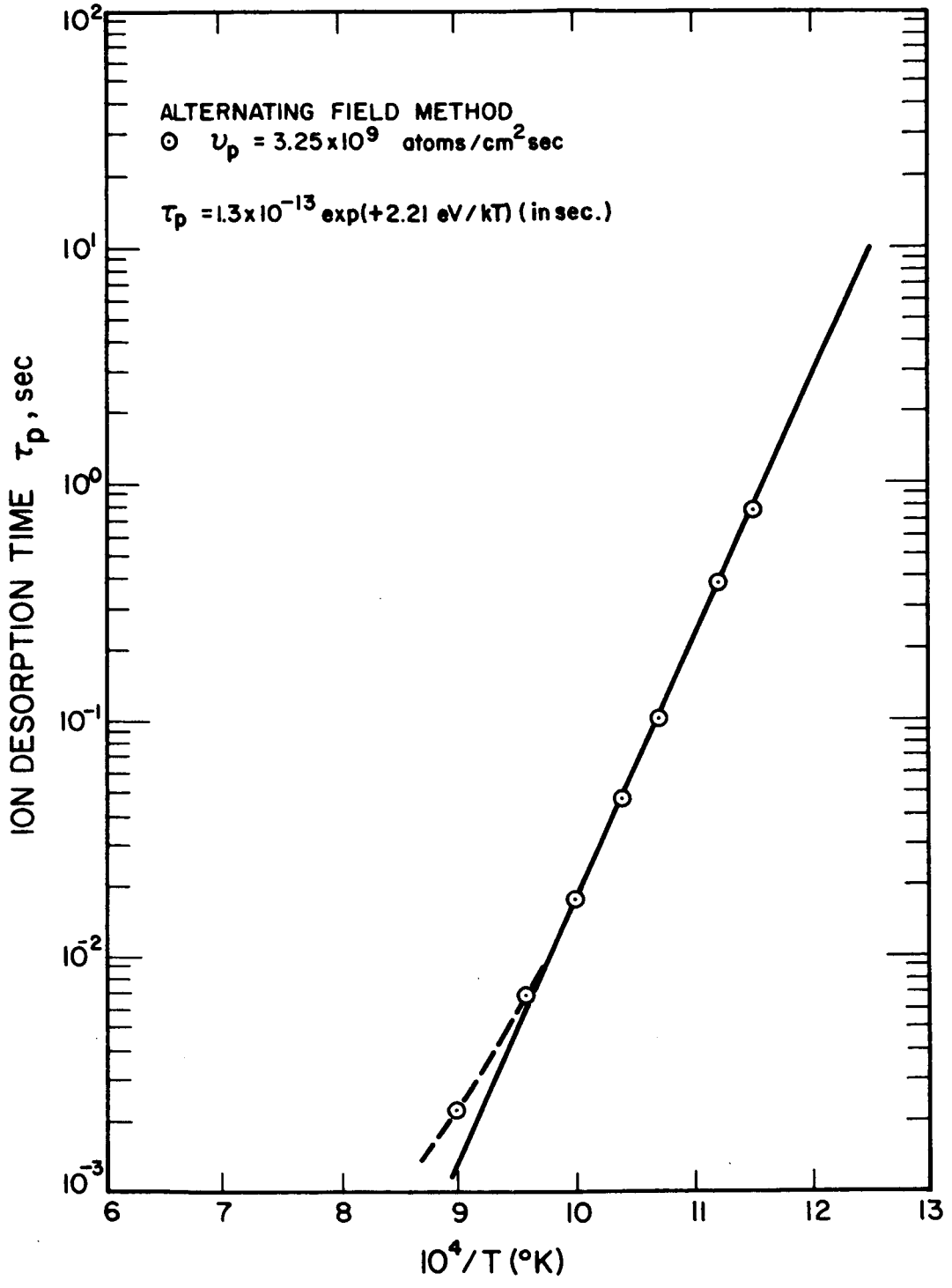


FIG. 9 $Cs^+$ DESORPTION TIME VS 1/T FOR A 74% W-26% Re ALLOY

their $I_p$ by that from the tungsten wire, before the background cesium flux became an appreciable fraction of the beam flux. Values for iridium, rhodium, tungsten, and the two alloys were obtained by the alternating field method, in which the level of the background flux is immaterial.

The first method of computation uses the desorption times of Tables 4 and 5 in the equation

$$\beta = \frac{1}{1 + (\tau_p/\tau_a)} , \tag{32}$$

which follows from the definition of $\beta$ and Eqs. 4 and 5. The second method makes use of the relation

$$\beta = \frac{1}{1 + 2 \exp [(\varphi - V_i)/kT]} \tag{33}$$

that results from the definition of $\beta$ and the Saha-Langmuir equation (Eq. 11) for cesium. $V_i$ is the ionization potential, again 3.893eV, and $\varphi$ is the work function. The value of $\beta$ in Table 7 is calculated for both Richardson and effective work functions, Tables 1 and 2 respectively.

TABLE 7

CESIUM IONIZATION EFFICIENCY FOR VARIOUS REFRACTORY MATERIALS AT 1000°K

| Material | Reference | Measured | Computed using $\tau_a, \tau_p$ (%) | Computed using $\varphi$** (%) | Computed using $\varphi_e$ (%) |
|---|---|---|---|---|---|
| Iridium | Present Work | 97±2 | | 96 | 97 |
| Rhenium | Present Work | 102±2 | | 100 | 100 |
| Rhodium | Present Work | 99.63±.10 | | 100 | 100 |
| Tantalum | Present Work | 87±2 | | 87 | 96 |
| Tungsten | Present Work | 99.99±.10 | 99.995 | 100 | 100 |
| | Ref. 3 | 100 | | | |
| 10%W-90%Ta | Present Work | 99.97±.10 | 99.973 | 99 | 100 |
| 74%W-26%Re | Present Work | 99.97±.10 | 99.972-99.990 | 100 | 100 |

The error for the measured β in the case of rhodium, tungsten and the alloys is a systematic error, whose evaluation can be found in Appendix D. In this instance the systematic error is 0.10 percent versus a 0.05 percent random error. For irridium the random error was much larger, hence this is the error reported. The larger random error for iridium is believed to be one consequence of the contamination effect mentioned in Subsection 3.3.4. Incidentally, our measured β of 97 percent for iridium is consistent with our measured work function, 4.22 or 4.24 eV (Table 1 or 2), and not with the literature values, 5.4[8] or 5.3 eV[9].

In the case of the tungsten-rhenium sample, increasing the accumulation time from 2 minutes to the 10 minutes required to reach a steady state coverage increased the β from 99.983 percent to 99.987 percent. This difference is much less than the systematic error, 0.100 percent. Since the time to reach a steady state coverage increases with decreasing temperature, the error due to a nonuniform coverage would increase. However, the change would be still much less than the systematic error.

## 4. CONCLUSION

A cesium beam experiment was conducted to study adsorption and desorption of cesium from the refractory materials iridium, rhenium, rhodium, tantalum, tungsten, 10 percent tungsten-90 percent tantalum, and 74 percent tungsten-26 percent rhenium. For these materials, electron work functions, critical temperatures, ion and atom adsorption lifetimes, ion and atom desorption energies, and ionization efficiencies were obtained. The data were taken under conditions of ultrahigh vacuum, $10^{-9}$ torr and lower. A residual gas analyzer was used to monitor the background gases and assess their composition. Critical temperatures by the beam technique were not as well defined as one might desire. However, further study is warranted before the technique is rejected for such high coverage phenomena. For low coverage phenomena, the suitability of the beam technique was well established both here and elsewhere.

The results are summarized in terms of three parameters that were evaluated. In each case, the more desirable materials are given first. The most important parameters for surface ionization engines are critical temperature and neutral fraction. The study indicated the order of increasing critical temperature to be

$$\text{Ir} < \text{Rh} < \text{Re, W} < \text{Alloys} < \text{Ta}$$

and the order of decreasing work function to be

$$\text{Rh} > \text{Re} > \text{W} > \text{W-Re} > \text{W-Ta} > \text{Ir} > \text{Ta.}$$

When ordered as to decreasing ionization efficiency $\beta$,

$$\text{Re} > \text{W} > \text{Alloys} > \text{Rh} > \text{Ir} > \text{Ta.}$$

In dealing with high-efficiency materials, it is often more convenient to speak of the neutral fraction $\alpha$. Since $\alpha + \beta = 1$, the last inequality is also in the order of increasing neutral fraction.

Four conclusions are deduced from the above inequalities:

1. The work function obtained for our iridium sample disagrees with values obtained by other investigators; however, it is consistent with the measured ionization efficiency.

2. Rhenium is better than tungsten as an ionizer material.

3. Rhodium is better than tungsten as an ionizer material. It has a lower critical temperature ($740^{\circ}K$) than rhenium, a higher effective work function (4.98 eV), and a high ionization efficiency (99.63 percent). From its work function value and by Eq. 33, nearly 100-percent efficiency was expected. However, in our opinion 100-percent efficiency was not obtained, because rhodium is more susceptible to gas contamination than rhenium or tungsten. Consistent with this conclusion was the fact that the curves, corresponding to Fig. 5, deviated much more from the expected exponential decay for rhodium than for rhenium or tungsten.

4. Whether or not, or how much, cesium surface ionization on rhodium is sensitive to gas contamination is a point worth pursuing. This is especially true if one desires to make use of rhodium's low critical temperature for lower power requirements than those for tungsten. Thus, we also recommend that the effects of gas contamination on cesium surface ionization be considered for future studies.

PREPARATION AND MEASUREMENT PROCEDURES

APPENDIX A — VACUUM CONDITIONING PROCEDURE

APPENDIX B — RESIDUAL BACKGROUND GAS DETERMINATION

APPENDIX C — TEMPERATURE CALIBRATION

APPENDIX D — ESTIMATE OF SYSTEMATIC ERRORS

APPENDIX E — CHEMICAL ANALYSIS

## APPENDIX A

## VACUUM CONDITIONING PROCEDURE

The procedure finally adopted as being the most successful for removing unwanted cesium from the vacuum chamber was to bake the system and liquid nitrogen trap to 150°C overnight while keeping the diffusion pump and foreline warm, and to pump with only the mechanical pump through the cold foreline trap, which collects the cesium for disposal. The chamber was then opened to change specimens. Ultrahigh vacuum was obtained by baking the liquid nitrogen trap and vacuum chamber to 150°C overnight while pumping with just the mechanical pump, then adding liquid nitrogen to the trap, after which the diffusion pump was started. The vacuum chamber was baked for another day before it was allowed to cool to room temperature. After several subsequent days of pumping, the vacuum chamber reached the $10^{-10}$ torr region.

## APPENDIX B

## RESIDUAL BACKGROUND GAS DETERMINATION

Base total pressure at the time of electron emission was about $1 \times 10^{-9}$ torr or less. Using a General Electric residual gas analyzer, the mass spectra of Figs. B-1 and B-2 were obtained. It is evident that the major constitutents of this background gas are diatomic hydrogen, water, carbon monoxide, or diatomic nitrogen. A thorough quantitative analysis requires a calibration of the mass spectrometer by introducing known quantities of various known gases into the spectrometer tube. This is necessary because most polyatomic gases fragment under electron bombardment, giving rise to a "cracking pattern" for that particular gas. Furthermore, this cracking pattern is, to a certain extent, dependent upon pressure and filament temperature.

After the electron emission measurements, the ampule supplying cesium to the chamber was broken. For the three runs made, the pressure surges on breaking the ampule varied from $10^{-8}$ to $10^{-7}$ torr with increases in the 14, 15, 16, and 28 peaks. From two of these three ampules there were also smaller increases in the 26 to 30 mass range and 37 to 44 mass range. For the other ampule, large peaks occurred at 20, 39, or 40 and 44. All the ampules were vacuum packed by the Dow Chemical Company and certified 99.97 percent pure. Nevertheless, after a period of pumping which varied from a day to several days, the residual background vacuum returned to the low $10^{-10}$ torr range and mass spectra similar to Figs. B-1 and B-2 were again obtained.

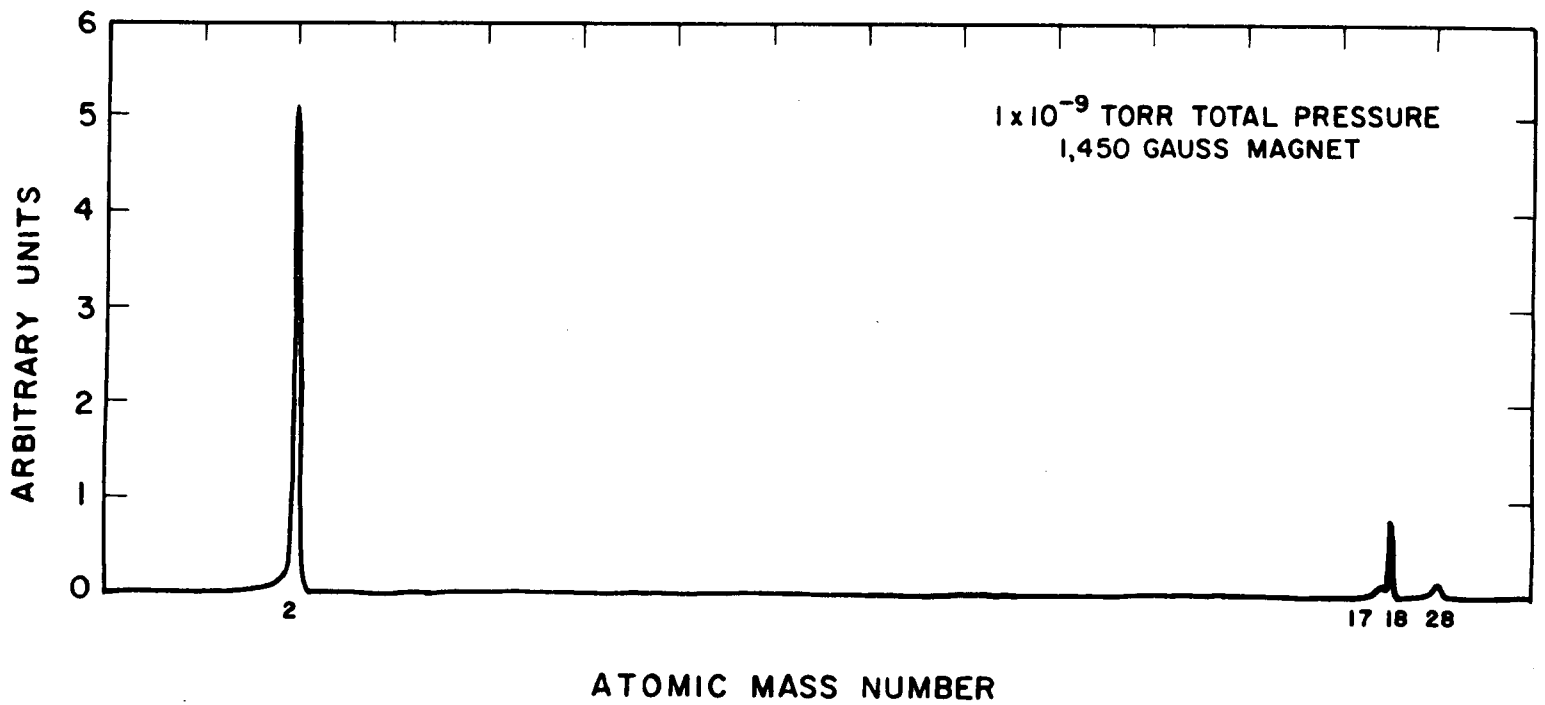


FIG. B-1 RESIDUAL GAS SPECTRUM, 2-28 AMU PEAKS

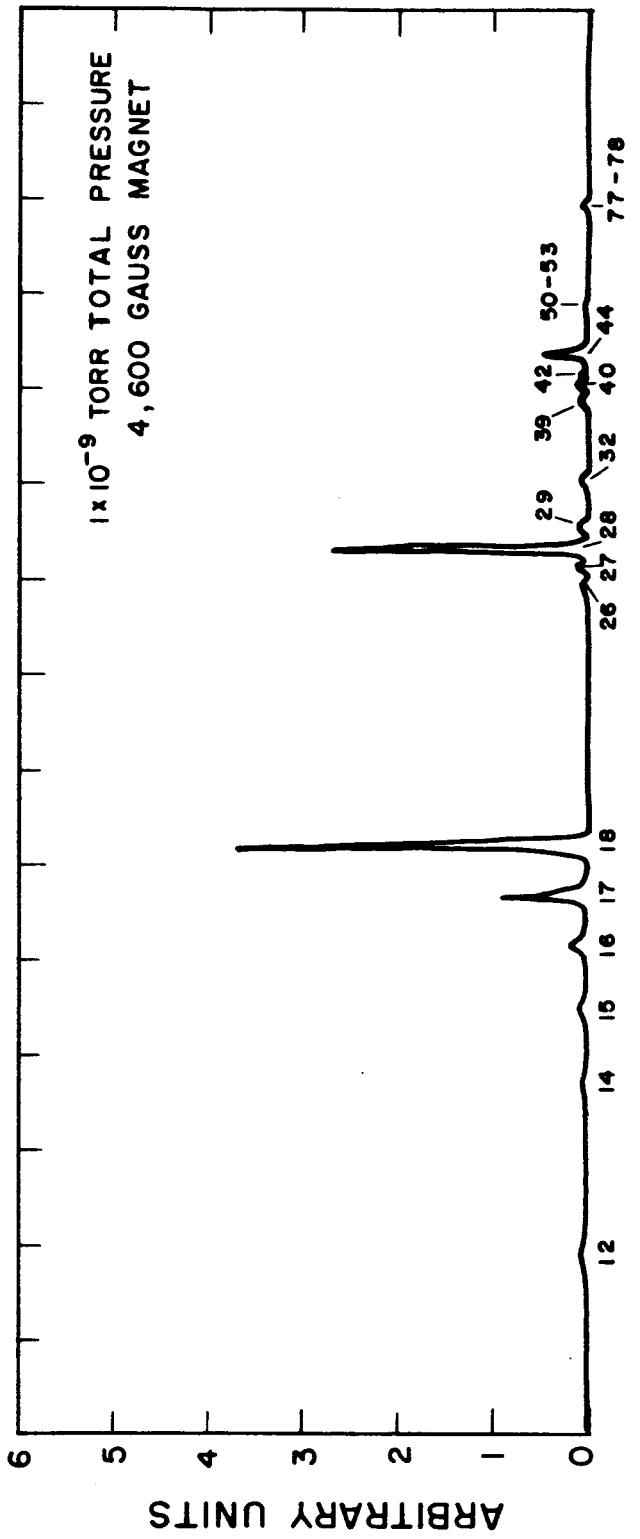


FIG. B-2 RESIDUAL GAS SPECTRUM, 12-78 AMU PEAKS

## APPENDIX C
## TEMPERATURE CALIBRATION

A Pyro Micro-Optical pyrometer was used to measure the filament surface temperature. Correcting for light absorption of the view port[22], this brightness temperature was then related to the desired bulk or true temperature of the filament by the expression

$$S = T\,(1 + 0.0452 \times 10^{-3}\, T \ln \epsilon_\lambda), \qquad T < 10^4\ ^\circ K \qquad \text{(C-1)}$$

which is the Wien's radiation law solved for the brightness temperature S. $\epsilon_\lambda$ is the spectral emissivity, which, because of the filter in the optical pyrometer, should be at 0.65 micron wavelength. Table C-I lists the values of $\epsilon_\lambda$ at 0.65 micron wavelength used for various materials, except for tantalum. In the case of tantalum only $\epsilon_\lambda$ values at 0.66 micron wavelength were found in the literature. We estimate, however, that the error in using $\epsilon_{0.66\mu}$ instead of $\epsilon_{0.65\mu}$ amounts to about 0.01 in $\epsilon_\lambda$ or 27°K difference in the temperature at 3,000°K.

No values of emissivity were available for the 10 percent tungsten-90 percent tantalum alloy. Because of the many similarities in properties of tantalum to tungsten, the tungsten calibration curve was used as an estimate for this alloy.

TABLE C-I

BRIGHTNESS VERSUS TRUE TEMPERATURE

| Material | Reference | True Temp. ($^{o}$K) | $\varepsilon_{0.65\mu}$ | Observed Temp* ($^{o}$K) |
|---|---|---|---|---|
| Iridium | Ref. 8 | 1000 | 0.411 | 958 |
| | | 1500 | 0.389 | 1394 |
| | | 2000 | 0.370 | 1805 |
| | | 2500 | 0.354 | 2195 |
| Rhenium | Ref. 23 | 1000 | 0.432 | 958 |
| | | 1500 | 0.423 | 1401 |
| | | 2000 | 0.414 | 1825 |
| | | 2500 | 0.405 | 2223 |
| | | 3000 | 0.395 | 2581 |
| Rhodium | Ref. 24 | 1000 | 0.272 | 939 |
| | | 1200 | 0.236 | 1103 |
| | | 1400 | 0.206 | 1256 |
| | | 1600 | 0.182 | 1393 |
| | | 1800 | 0.165 | 1526 |
| Tantalum (0.66$\mu$) | Ref. 25, 26 | 1000 | 0.459 | 963 |
| | | 1500 | 0.438 | 1408 |
| | | 2000 | 0.419 | 1828 |
| | | 2500 | 0.401 | 2218 |
| | | 3000 | 0.385 | 2578 |
| Tungsten | Ref. 27 | 1000 | 0.458 | 963 |
| | | 1500 | 0.448 | 1411 |
| | | 2000 | 0.438 | 1843 |
| | | 2500 | 0.428 | 2256 |
| | | 3000 | 0.418 | 2648 |
| | | 3500 | 0.408 | 3336 |
| 10 percent W-90 percent Ta | | See text | | |
| 74 percent W-26 percent Re | Ref. 28 | 1000 | 0.627 | 990 |
| | | 1200 | 0.617 | 1170 |
| | | 1400 | 0.605 | 1355 |
| | | 1600 | 0.595 | 1535 |
| | | 1800 | 0.587 | 1720 |
| | | 2000 | 0.578 | 1900 |

*Corrected for light attenuation by a plane window.

## APPENDIX D

## ESTIMATE OF SYSTEMATIC ERRORS

In order to make a simple estimate of the systematic errors, the technique of linear addition of partial differentials is employed.

For example, to estimate the systematic error in the true temperature T because of inaccuracies in the emissivity $\epsilon$ or the pyrometer temperature S, consider Wein's radiation law

$$\ln \epsilon_\lambda = \frac{C_2}{\lambda} \left( \frac{1}{T} - \frac{1}{S} \right). \tag{D-1}$$

Solving for T, we have

$$T = \frac{C_2 S}{\lambda S \ln \epsilon_\lambda + C_2} . \tag{D-2}$$

Then compute $\Delta T/T$ for variations in S and $\epsilon_\lambda$, to find that

$$\frac{\Delta T}{T} = \frac{\Delta S}{S} + T \frac{\lambda}{C_2} \left( \frac{\Delta S}{S} \ln \epsilon_\lambda + \frac{\Delta \epsilon}{\epsilon} \right) , \tag{D-3}$$

into which was substituted $C_2$ = 14,380 micron degrees and $\lambda$ = 0.65 microns. The maximum temperature of interest is 2,100°K and the Pyro Micro-Optical pyrometer is accurate to 1 percent. We expect $\Delta\epsilon/\epsilon$ to have been no greater than 10 percent and in most cases less. The resulting $\Delta T/T$ is about 2 percent.

The systematic error in $\varphi^{**}$ is found by taking partial differentials of I, a, and T for Eq. 1, where we have set J = I/a, a being the area of the filament that the collector sees and I the collector current as read by a meter. The result is

$$\frac{\Delta \varphi^{**}}{\varphi^{**}} = \frac{\Delta T}{T} + kT \left( \frac{\Delta I}{I} + \frac{\Delta a}{a} + \frac{2\Delta T}{T} \right) . \tag{D-4}$$

The current meter used has a 4 percent error and $\Delta a/a$ is approximately 10 percent maximum, hence for a 10 percent error in emissivity, we have a 2.7 percent error in $\Delta\varphi^{**}/\varphi^{**}$. The maximum temperature is as before.

To find the systematic error in $Q_p$ of Eq. 20, take partial differentials of T and $\tau_p$, i.e.

$$\frac{\Delta Q_p}{Q_p} = \frac{dT}{T} \ln Q_p + kT \frac{\Delta \tau_p}{\tau_p} \qquad \text{(D-5)}$$

The maximum $Q_p$ measured was 3.25 eV for temperatures up to about 1,000°K. Above this temperature the data were not included for evaluation of the slope to find $Q_p$. The oscilloscope is 3 percent accurate, hence one might have a maximum error of 12 percent in determining $\tau_p$ from the trace (2 measurements of length). The result is 0.34 percent error for $\Delta Q_p/Q_p$.

The systematic error in $\beta$, as determined by the alternating field method, is evaluated by taking partial differentials of $I_o$ and $I_\infty$ in Eq. 31. The result is

$$\frac{\Delta\beta}{\beta} = \frac{(\Delta I_o/I_o) - (\Delta I_\infty/I_\infty)}{(I_o/I_\infty) - 1} \qquad \text{(D-6)}$$

Since $I_o$ is an oscilloscope trace, $\Delta I_o/I_o$ is 6 percent. $I_\infty$ is read from a Keithley 600A electrometer, having a 4 percent calibration. For tungsten and the two alloys, we found $I_o/I_\infty$ to be a minimum of 100 for the range of temperature used to evaluate $\beta$ and $Q_p$, hence $\Delta\beta/\beta$ is 0.1 percent for these three materials. Iridium had a $I_o/I_\infty$ of 50, hence its systematic error in $\Delta\beta/\beta$ was 0.2 percent.

## APPENDIX E
## CHEMICAL ANALYSIS

In most cases it was neither practical nor possible to obtain a quantitative spectroanalysis of the wire specimens. Consequently, except for the 10 percent tungsten-90 percent tantalum specimen, all are semiquantitative analyses of the pretreated wire in Table E-I. Since a semiquantitative analysis is not sufficiently sensitive to reveal differences between the pretreated and treated wire, no analyses were performed on the treated wire.

TABLE E-I

SPECTROGRAPHIC ANALYSIS

Iridium wire (Ir)

| | |
|---|---|
| Iridium - | remainder |
| Copper- | 0.00064% |
| Calcium- | trace |
| less than 0.0002 | |
| Rhodium- | 0.058 |
| Platium- | 0.024 |
| Other elements- | nil |

Rhenium wire (Re)

| | |
|---|---|
| Rhenium- | remainder |
| Calcium- | trace |
| less than 0.0005% | |
| Iron- | 0.0072 |
| Silicon- | 0.012 |
| Other elements- | nil |

Rhodium wire (Rh)

| | |
|---|---|
| Rhodium- | remainder |
| Calcium- | 0.0017% |
| Copper- | 0.00060 |
| Iron- | 0.070 |
| Boron- | 0.032 |
| Chromium | 0.0068 |
| Other elements- | nil |

Tantalum wire (Ta)

| | |
|---|---|
| Tantalum- | remainder |
| Silicon- | 0.0070% |
| Copper- | 0.0032 |
| Other elements- | nil |

Tungsten wire (W)

| | |
|---|---|
| Tungsten- | remainder |
| Silicon- | 0.017% |
| Magnesium- | trace |
| less than 0.0003 | |
| Iron- | trace |
| less than 0.006 | |
| Copper- | 0.0011 |
| Calcium- | trace |
| less than 0.0004 | |
| Other elements- | nil |

74% Tungsten-26% Rhenium

| | |
|---|---|
| Tungsten- | remainder |
| Rhenium- | 32.% * |
| Calcium- | trace |
| less than 0.0004 | |
| Silicon- | not detected |
| less than 0.009 | |
| Magnesium- | trace |
| less than 0.0003 | |
| Copper- | 0.00076 |
| Other elements- | nil |

10% Tungsten-90% Tantalum

| | | | |
|---|---|---|---|
| C | 20 ppm | Ni | less than 10 ppm |
| H | 5 ppm | Ti | less than 10 ppm |
| O | 640 ppm | Zr | less than 10 ppm |
| Cb | 800 ppm | Cr | less than 10 ppm |
| Fe | 50 ppm | Mg | less than 10 ppm |
| Mo | 50 ppm | Mn | less than 10 ppm |
| Si | 50 ppm | V | less than 10 ppm |
| Ca | 10 ppm | Sn | less than 50 ppm |
| Al | less than 10 ppm | W | 10.1% |
| | | Tantalum | balance |

*Major constituents are only approximate in a semiquantitative analysis.

## REFERENCES


1. Electro-Optical Systems, Inc., Surface Ionization Studies, by D. Zuccaro, EOS 2130-Final, Contract NAS8-2546, Pasadena, Calif., Dec 1963

2. Electro-Optical Systems, Inc., Surface Ionization Studies, by W. D. Dong, D. G. Worden, and D. Zuccaro, Contract NASA CR-54047, Pasadena, Calif., Jun 1964

3. S. Datz and E. H. Taylor, "Ionization on Platinum and Tungsten Surfaces, I. The Alkali Metals," J. Chem. Phys., Vol. 25, Sep 1956, pp. 389-394

4. S. V. Starodubtsev, "Application of the Method of Modulated Molecular Beams for the Study of Adsorption Phenomena," Soviet Phys.--JETP, Vol. 19, 1949, pp. 215-224

5. R. C. Evans, "The Positive Ion Work Function of Tungsten for the Alkali Metals," Proc. Roy. Soc. (London), Vol. A139, 1933, pp. 604-617

6. F. L. Hughes and H. Levinstein, "Mean Adsorption Lifetime of Rb on Etched Tungsten Single Crystals: Ions," Phys. Rev., Vol. 113, 1959, pp. 1029-1035

7. E. B. Hensley, "Thermionic Emission Constants and Their Interpretation," J. Appl. Phys., Vol. 32, Feb 1961, pp. 301-308

8. D. L. Goldwater and W. E. Danforth, "Thermionic Emission Constants of Iridium," Phys. Rev., Vol. 103, Aug 1956, pp. 871-872

9. O. A. Weinreich, "Thermionic Properties of Uncoated and Thoria-Coated Rhodium and Iridium Cathodes," Phys. Rev., Vol. 82, 1951, p. 573

10. Electro-Optical Systems, Inc., Ionizer Development and Surface Physics Studies, by L. H. Taylor and H. H. Todd, EOS 1660/1-IR-1, Contract NAS8-1537, Pasadena, Calif., Sep 1962

11. R. Levi and G. A. Espersen, "Preparation of Rhenium Emitters and Measurements of Their Thermionic Properties," Phys. Rev., Vol. 78, May 1950, pp. 231-234

12. C. Agte, H. Alterthum, K. Becker, G. Heyne, and K. Moers, "Physical and Chemical Properties of Rhenium," Z. Anorg. Allgem. Chem., Vol. 196, 1931, pp. 129-159

13. H. B. Wahlin and L. V. Whitney, "Temperature Scale and Thermionic Emission from Rhodium," J. Chem. Phys., Vol. 6, 1938, p. 594

14. M. D. Fiske, "The Temperature Scale, Thermionics and Thermatomics of Tantalum," Phys. Rev., Vol. 61, p. 513, 1942

15. A. L. Riemann, Phil. Mag., Vol. 25, 1938, p. 834

16. J. B. Taylor and I. Langmuir, "The Evaporation of Atoms and Ions from Cesium Films on Tungsten," Phys. Rev., Vol. 44, Sep 1933, pp. 423-458

17. D. G. Worden, "The Effects of Surface Structure and Adsorption on the Ionization Efficiency of a Surface Ionization Source," Progress in Astronautics and Rocketry, Vol. 5, New York, Academic Press, 1961

18. I. Langmuir and K. H. Kingdom, "Thermionic Effects Caused by Vapours of Alkali Metals," Proc. Roy. Soc. (London), Vol. A107, 1925, pp. 61-79

19. F. Knauer, Z. Physik, Vol. 125, 1948, p. 278

20. M. D. Scheer and J. Fine, "Kinetics of $Cs^+$ Desorption from Tungsten", J. Chem. Phys., Vol. 37, Jul 1962, pp. 107-113

21. American Institute of Physics Handbook, New York, McGraw-Hill, 1957, p. 7-14

22. Pyrometric Practice, by P. D. Foote, C. O. Fairchild, and T. R. Harrison, Bureau of Standards Technical Publication 170, 1921

23. D. T. Marple, "Special Emissivity of Rhenium", J. Opt. Soc. Am., Vol. 46, Jul 1956, pp. 490-494

24. A. Goldsmith, T. E. Waterman, and H. J. Hirschhorn, Thermophysical Properties of Solid Materials, Rev., New York, MacMillan, 1961, p. 555

25. C. J. Smithells, Metals Reference Book, Vol. II, London, Butterworths

26. M. Davis and J. F. Duke, "An Investigation Into the Possibility of Fabricating Rhenium Metal", Services Electronics Research Lab Tech. J., Vol. 6, Aug 1956, pp. 65-78

27. Handbook of Physics and Chemistry, 41st Edition

28. Electro-Optical Systems, Inc., Applied Research on Contact Ionization Thrustor, by S. L. Eilenberg, EOS 4800-M-7, Contract AF 33(615)-1530, Pasadena, Calif., 29 Nov 1964

DISTRIBUTION LIST FOR FINAL REPORT
CONTRACT NAS3-5244

1. NASA-Lewis Research Center
Spacecraft Technology Procurement Section
21000 Brookpark Road
Cleveland, Ohio 44135
Attention: John H. DeFord — 1

2. NASA-Lewis Research Center
Technology Utilization Office
21000 Brookpark Road
Cleveland, Ohio 44135
Attention: John Weber — 1

3. NASA-Marshall Space Flight Center
Huntsville, Alabama
Attention: M-RP-DIR/Dr. E. Stuhlinger — 1

4. NASA Headquarters
FOB - 10B
600 Independence Avenue, N. E.
Washington, D. C. 20546
Attention: RNT/James Lazar — 2

5. Commander
Aeronautical Systems Division
Wright-Patterson Air Force Base, Ohio
Attention: AFAPL (APIE)/Lt. Robert Supp — 1

6. Jet Propulsion Laboratory
4800 Oak Grove Drive
Pasadena, California
Attention: J. J. Paulson — 1

7. Field Emission Corporation
McMinnville, Oregon
Attention: L. W. Swanson — 1

8. General Electric Company
Flight Propulsion Lab.
Cincinnati, Ohio 45215
Attention: M. L. Bromberg — 1

9. Ion Physics Corporation
Burlington, Massachusetts
Attention: Dr. S. V. Nablo — 1

10. Space Technology Laboratories
8433 Fallbrook Avenue
Canoga Park, California
Attention: Dr. D. Langmuir — 1

11. North American Aviation, Inc.
12214 Lakewood Avenue
Downey, California
Attention: Technical Information Office
Dept. 4096-314 — 1

12. NASA-Lewis Research Center
21000 Brookpark Road
Cleveland, Ohio 44135
Attention: Library — 2

13. Aerojet-General
Nucleonics Division
San Ramon, California
Attention: Mr. J. S. Luce — 1

14. Hughes Research Laboratories
Malibu Canyon Road
Malibu, California
Attention: Dr. G. R. Brewer — 1

15. NASA-Lewis Research Center
Spacecraft Technology Division
21000 Brookpark Road
Cleveland, Ohio 44135
Attention: J. H. Childs — 2
Y. E. Strausser — 7

16. United Aircraft Corporation
Research Department
East Hartford, Connecticut
Attention: Dr. R. G. Meyerand, Jr. — 1

17. TRW Electromechanical Division
Thompson Ramo Wooldridge, Inc.
23555 Euclid Avenue
Cleveland, Ohio 44117
Attention: R. T. Craig — 1

18. NASA-Lewis Research Center
Electromagnetic Propulsion Division
21000 Brookpark Road
Cleveland, Ohio 44135
Attention: R. Breitwieser 1
W. Moeckel 1
E. A. Richly 1

19. Westinghouse Astronuclear Laboratories
Pittsburgh, Pennsylvania 15234
Attention: Electric Propulsion Laboratory 1
Mr. W. H. Szymanowski 1

20. NASA Scientific and Technical Information Facility
Box 5700
Bethesda, Maryland 20014
Attention: RQT-2448/NASA Representative 6

21. AFWL
WLPC/Capt. C. F. Ellis
Kirtland Air Force Base
New Mexico 1

22. NASA-Lewis Research Center
21000 Brookpark Road
Cleveland, Ohio 44135
Attention: Reports Control Office 1

23. Aerospace Corporation
P. O. Box 95085
Los Angeles, California 90045
Attention: Library Technical Documents Group 1